J. Astron. Space Sci. 16(2), 91–104 (1999)

# COLOR GRADIENT IN THE KING TYPE GLOBULAR CLUSTER NGC 7089

**Young-Jong Sohn[1], Mun-Suk Chun[2], Jae-Woo Lee[3], and Jungmin Oh[2]**
[1]Center for Space Astrophysics, Yonsei University, Seoul 120-749, Korea
[2]Department of Astronomy, Yonsei University, Seoul 120-749, Korea
[3]Department of Physics and Astronomy, University of North Carolina, Chapel Hill, NC 27599-3255, USA

*(Received April 1, 1999; Accepted May 15, 1999)*

## ABSTRACT

We use $BV$ CCD images to investigate the reality of the color gradient within a King type globular cluster NGC 7089. Surface photometry shows that there is a strong radial color gradient in the central region of the cluster in the sense of bluer center with the amplitude of $\sim 0.39 \pm 0.07$ mag/arcsec$^2$ in $(B-V)$. In the outer region of the cluster, however, the radial color gradient shows a reverse case, i.e., redder toward the center. $(B-V)$ color profile which was derived from resolved stars in NGC 7089 field also shows a significant color gradient in the central region of the clusters, indicating that lights from the combination of red giant stars and blue horizontal branch stars cause the radial color gradient. Color gradient of the outer region of NGC 7089 may be due to the unresolved background of the cluster. Similar color gradients in the central area of clusters have been previously observed exclusively in highly concentrated systems classified as post core collapse clusters. We caution, however, to confirm the reality of the color gradient from resolved stars, we need more accurate imaging data of the cluster with exceptional seeing condition because the effect of completeness correlates with local density of stars.

## 1. INTRODUCTION

The radial color and population gradients in a globular cluster may occur as results of dynamical evolution of the system. The energy equipartition, which leads a mass segregation phenomenon, sinks more massive stars toward the cluster center. There are evidences that the morphology of the local mass function varies along the radius within a cluster (Bolte 1989, Richer & Fahlman 1989, Drukier et al. 1993). Close stellar encounters may also help to make massive objects such as blue stragglers or binary stars in denser central region of a globular cluster (Grindlay et al. 1984, Nemec & Harris 1987, Leonard 1989, Nemec & Cohen 1989).

Studies with direct CCD surface photometry and digital star counts have suggested that color gradients exist exclusively for the post core collapse (PCC) clusters in the sense of bluer center

(Djorgovski et al. 1988, Piotto et al. 1988, Djorgovski et al. 1991a, 1991b, Djorgovski & Piotto 1993). PCC clusters are usually characterized by a power law cusp in the central part of their surface brightness profiles, while traditional King (1966) type (KM) clusters have flat cores. Exceptionally, Sohn et al. (1996) found that a KM cluster NGC 7089 (M2) shows a remarkable color gradient in central region of the cluster bluering to the cluster center by the amplitude of $(B-V) \sim 0.1$ mag/arcsec$^2$. They also found similar color gradients in the central regions of the KM clusters NGC 6402 and NGC 6934. However, the crowding effect associated with relatively poor seeing conditions (FWHM $\sim 3''.7$) prevented them from sampling stellar populations with acceptable photometric accuracy.

In this paper, we used $BV$ CCD images of NGC 7089, which were obtained from 0.9m telescope at KPNO to investigate the reality of the color and population gradients in the cluster. NGC 7089 is a high latitude globular cluster [$\alpha = 21^h33^m, \delta = -0^o49'(2000); l = 53^o, b = -36^o$] with only a small amount of interstellar reddening, $E(B-V) = 0.02$ (Zinn 1985). Harris (1975), Auriere & Cordoni (1983), and Cudworth & Rauscher (1987) have published CMDs for the bright stars ($V < 18$ mag) based on the photographic photometry. Lee & Carney (1999) presented $BV$ CCD photometry data for 30 RR Lyrae variables and CMD of NGC 7089, which shows a very extended blue horizontal branch (HB) tail and no significant blue HB gaps. The observation, data reduction procedures, and standardization are described in Sec. 2. In Sec. 3, we describe the surface photometry and color gradient of NGC 7089. Stellar photometry and color gradient are presented in Sec. 4. In Sec. 5, the color gradient of NGC 7089 is discussed comparing with the other previous results. A summary of the results is given in Sec. 6.

## 2. OBSERVATION, DATA REDUCTION, AND STANDARDIZATION

$BV$ images of NGC 7089 were obtained during the night of UT 1998 September 1 using the 0.9m telescope at KPNO. The detector was T2KA CCD chip of 2048 × 2048 format. At the f/7.5 focus, the image scale is 0.68 arcsec pixel$^{-1}$, which gives the sky coverage of 23.5 × 23.5 arcmin$^2$. Exposure times were 360 and 240 seconds for $B$ and $V$, respectively. The seeing, as measured from the reduced images, is $\sim 1.8$ arcsec in $V$, and $\sim 1.9$ arcsec in $B$.

The data reduction followed standard processing lines. A median bias frame was subtracted from the raw exposures, and the results were then divided by dome flats to remove pixel to pixel variations. Illumination corrections using sky flats were also applied to eliminate the large scale structure. These procedures produced object frames flattened to better than 0.5% in both filters.

During the nights of 1998 August 31 and September 1, we observed 30 standard stars from the list of Landolt (1992) to derive the calibration coefficients. The standard star observations cover $(B-V)$ color range of 0.4 to 1.2, and $V$ of 11.2 to 15.3. The photometric transformations were assumed to have the following forms:

$$V - v_o = \epsilon(b-v)_o + \zeta_V \quad (1)$$

$$(B-V) = \mu(b-v)_o + \zeta_{B-V} \quad (2)$$

Our transformation coefficients are $\epsilon = -0.008 \pm 0.026$, $\zeta_V = -3.168 \pm 0.023$, $\mu = +1.095 \pm 0.024$, and $\zeta_{B-V} = -0.176 \pm 0.021$. Figure 1 shows the residuals of $(B-V)$ and $V$ for the selected standard stars.

## 3. SURFACE PHOTOMETRY AND COLOR GRADIENT

Surface brightness and radial color profiles of NGC 7089 have been derived applying techniques of Sohn et al. (1996). At first, we determined the accurate position of cluster center from the stellar distributions on $x-$ and $y-$ axis of the $B$ band cluster image. The positions of stars in the cluster image were measured from the point spread function (PSF) fitting stellar photometry, from which we find stellar magnitudes as well (see Sec. 4). The median and mean positions of stellar distribution in each axis are used to estimate the mode value, $3\times$median$-2\times$mean, which we adopted as center positions of each axis. The center position was double-checked by comparing the position determined from the CENTER task in IRAF, which was applied to the central area of the 20 pixels binned boxcur smoothed $B$ band image. We also examined the corresponding contour map and intensity profiles crossing the cluster center. Cluster center positions derived from all of these techniques are in good agreement each other. The accurate center position of $V$ band image was then derived from the coordinate transformation equation between the positions of stars on $B$ and $V$ images.

Particular attention was given to measure the accurate sky level of the cluster images. The size of the field of view ($\sim$ 23.5 arcmin) is large enough to cover NGC 7089 almost out to the tidal radius ($r_t \sim 14.8$ arcmin, see Sohn et al. 1996). Therefore, sky values of each bandpass image are estimated by measuring the mean intensity per unit area of four outer corner areas with $100 \times 100$ pixels.

The sky-subtracted cluster image is divided into eight sectors and concentric annuli of logarithmic radius increments. For each annulus, we define an effective radius $r_e = [\frac{1}{2}(r_1^2 + r_2^2)]^{1/2}$, where $r_1$ and $r_2$ are the inner and outer radii of annulus. The median value of the eight sector measurements is considered the local surface brightness at an effective radius. The corresponding error is based on the standard deviation of the median value. Note that taking the median value of eight sectors has almost the same effect as removing the bright foreground stars before applying the surface photometry, unless the size of the aperture is too small to be divided into eight sectors of meaningful size (Lee 1990). The resulting $B$ band median surface brightnesses and errors for NGC 7089 are listed in columns 2 and 3 of Table 1. The brightness distribution, having a flat core as shown in Figure 2, can be characterized by the isothermal King (1966) model. Sohn et al. (1996) derived the concentration parameter of NGC 7089 to be $c = log(r_t/r_c) = 1.65$, with which we derived the appropriate KM model profile and fitted to the observed surface brightness distribution of NGC 7089.

The annulus color was determined using the $B$ and $V$ median surface brightness values of eight sectors. The resulting median $(B-V)$ colors and errors are listed in columns 4 and 5 of Table 1. The errors are also the standard deviation to the median $(B-V)$ colors of the eight sector values. The upper panel of Figure 3 shows the radial $(B-V)$ color distribution of NGC 7089. Also shown in the lower panel of Figure 3 are the previousely compiled photoelectric measurements of Peterson (1986). Estimate for the slopes of radial color distributions inside and outside to $\log(r_e) = 1''.1$ has been made by weighted least square fits. We do not use the inner most point $\log(r_e) = 0''.260$,

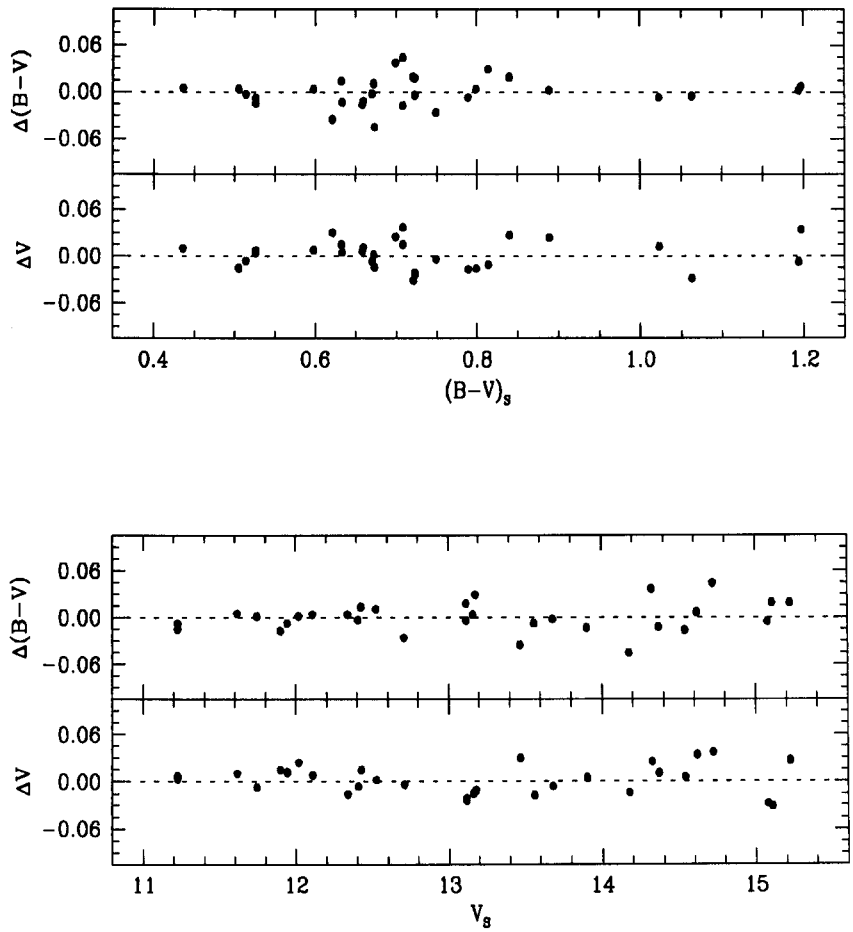


**Figure 1.** Transformation residuals of Landolt (1992) standard stars as functions of the color and magnitude. The differences are in the sense Landolt (1992) minus our work.

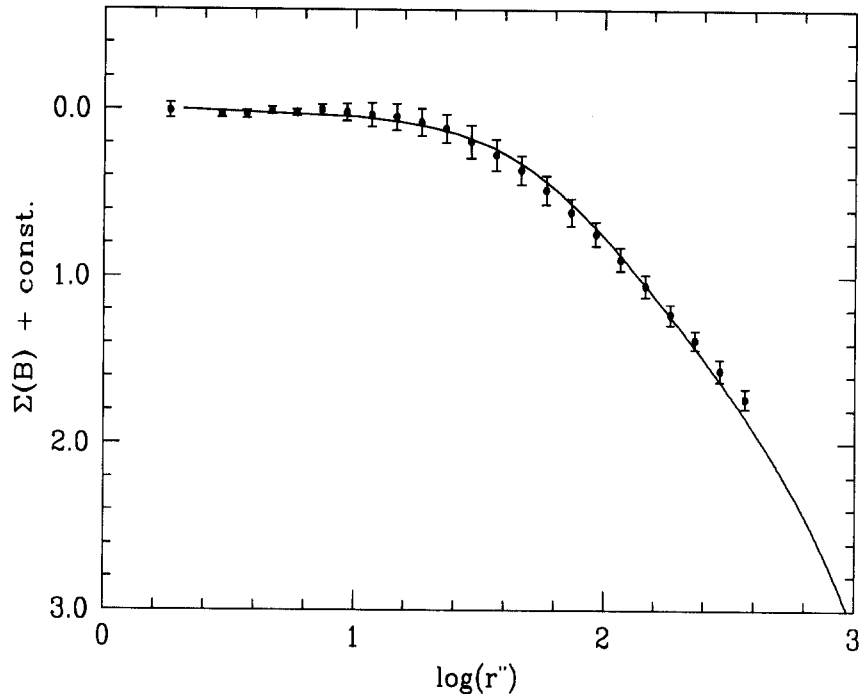


**Figure 2.** Surface brightness distribution of NGC 7089. An isothermal King (1966) model with $c = 1.65$ has been fitted to the observed surface brightness distribution.

inside of which are presumably under the effect of seeing. It is apparent that there is a strong radial color gradient in the central region of the cluster in the sense of bluer center with the amplitude of $\sim 0.39 \pm 0.07$ mag/arcsec$^2$, which is much steeper than the previous value ($0.12 \pm 0.07$ mag/arcsec$^2$) of Sohn et al. (1996). We note that the relatively shallower color gradient of Sohn et al. (1996) might be affected by the severe crowding effect caused from a poor seeing condition ($\sim 3''.7$). In the outer region of the cluster, however, the trend of radial color gradient is reversed, i.e., redder toward the center with the amplitude of $\sim -0.18 \pm 0.01$ mag/arcsec$^2$.

## 4. *BV* STELLAR PHOTOMETRY AND COLOR GRADIENT

Is the color gradient reported in Sec. 3 due to the resolved stellar distribution within the cluster, or

**Table 1.** Median annuli surface brightness and $(B-V)$ colors of NGC 7089.

| [1mm] $\log r_e''$ | $\Sigma(B)$ | $\sigma_{\Sigma(B)}$ | $(B-V)$ | $\sigma_{(B-V)}$ |
|---|---|---|---|---|
| 0.260 | -6.808 | 0.047 | 0.504 | 0.053 |
| 0.466 | -6.828 | 0.020 | 0.683 | 0.044 |
| 0.566 | -6.828 | 0.025 | 0.673 | 0.038 |
| 0.666 | -6.805 | 0.022 | 0.713 | 0.043 |
| 0.766 | -6.819 | 0.021 | 0.732 | 0.048 |
| 0.866 | -6.801 | 0.031 | 0.820 | 0.045 |
| 0.966 | -6.816 | 0.051 | 0.866 | 0.070 |
| 1.066 | -6.831 | 0.072 | 0.831 | 0.095 |
| 1.166 | -6.842 | 0.080 | 0.797 | 0.102 |
| 1.266 | -6.876 | 0.083 | 0.756 | 0.106 |
| 1.366 | -6.912 | 0.085 | 0.770 | 0.107 |
| 1.466 | -6.991 | 0.097 | 0.682 | 0.129 |
| 1.566 | -7.070 | 0.093 | 0.702 | 0.119 |
| 1.666 | -7.162 | 0.088 | 0.682 | 0.115 |
| 1.766 | -7.280 | 0.086 | 0.661 | 0.115 |
| 1.866 | -7.414 | 0.081 | 0.646 | 0.108 |
| 1.966 | -7.543 | 0.072 | 0.627 | 0.098 |
| 2.066 | -7.694 | 0.068 | 0.621 | 0.093 |
| 2.166 | -7.852 | 0.066 | 0.606 | 0.090 |
| 2.266 | -8.024 | 0.062 | 0.606 | 0.085 |
| 2.366 | -8.177 | 0.058 | 0.570 | 0.079 |
| 2.466 | -8.362 | 0.065 | 0.560 | 0.090 |
| 2.566 | -8.532 | 0.059 | 0.561 | 0.081 |

is it due to the unresolved background of the cluster image, which is mostly composed of faint stars? PSF-fitting photometry can be used to answer this question, because it separated the background image to the measeured stellar images. The $B$ and $V$ magnitudes of individual stars in NGC 7089 were measured with the PSF-fitting program ALLSTAR (Stetson & Harris 1988), which is part of DAOPHOT (Stetson 1987) photometry package. To calculate the point spread functions, we use $\sim$ 80 isolated bright stars located at radii larger than 500 pixels from the cluster center, within which stars can be affected by the crowding effect. An iterative method had been applied to remove neighboring faint stars of selected PSF stars, so that we were able to achieve appropriate PSFs for each frame. Total 9,934 stars were detected in both $B$ and $V$ images of NGC 7089. Apperture corrections, which were estimated from comparison of the PSF magnitudes and the integrated magnitudes from the growth-curve method to PSF stars, extinction corrections, and finally photometric transformations were then applied to derive the standard magnitudes of stars in each image. $(B-V)$ and $V$ color

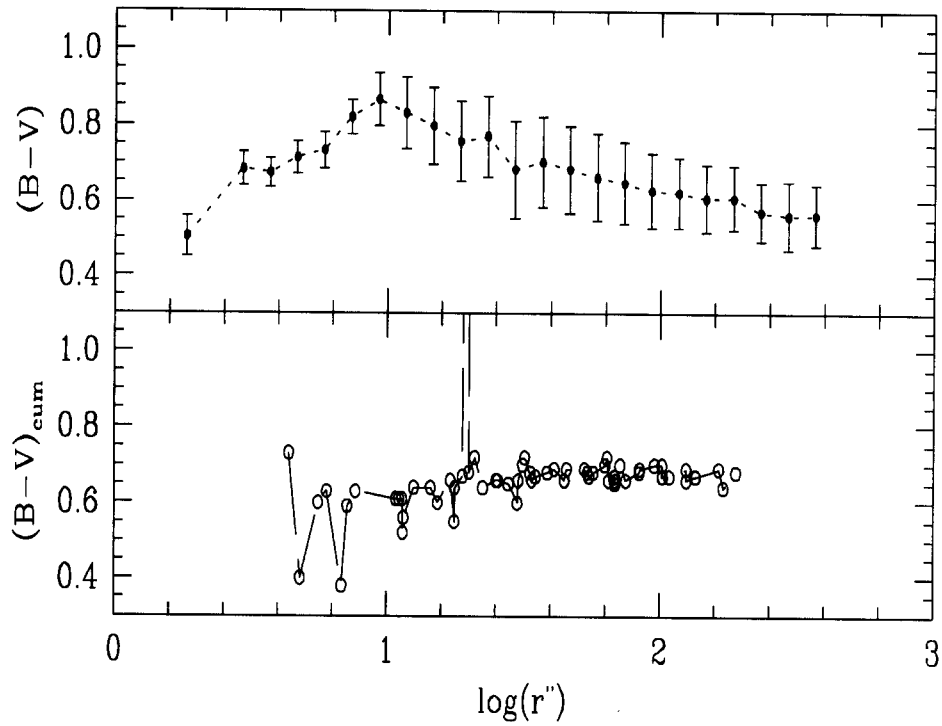


**Figure 3.** Radial $(B-V)$ color distribution within NGC 7089. The local annuli colors are shown in the upper panel. In the lower panel, the photoelectric measurements compiled by Peterson (1986) are shown for comparison.

magnitude diagram of stars in NGC 7089 having $\chi < 1.3$ is shown in Figure 4. Here, $\chi$ is a estimate of ratio: the observed pixel-to-pixel scatter from the model image profile devided by the expected pixel-to-pixel scatter from the image profile (Stetson 1995).

Using the $B$ and $V$ magnitudes of resolved stars on the NGC 7089 field, we derived the radial $(B-V)$ color profile with the same radius ranges applied to the surface phtometry (Sec. 3), and illustrated it in the upper panel of Figure 5. The resulting radial $(B-V)$ colors and errors of resolved stars are listed in columns 2 and 3 of Table 2. As seen in the figure, a strong color gradient appears in the central region of the cluster, while it is apparent that there is no significant color gradient outside of NGC 7089.

We also applied the surface photometry to the star-subtracted $B$ and $V$ images, which were produced from DAOPHOT/ALLSTAR run. Same as the surface photometry to the observed $B$

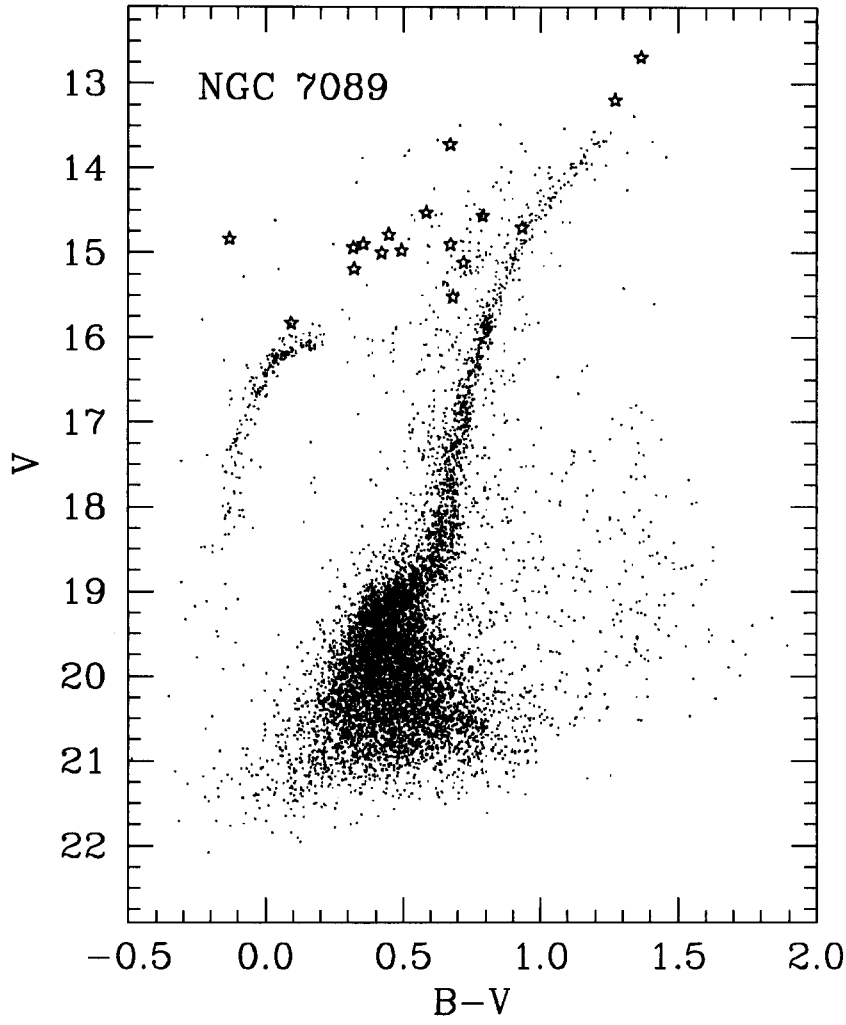


**Figure 4.** The resulting $(B - V)$ and $V$ color magnitude diagram of NGC 7089. Star-like symbols indicate bright stars resolved in the central region ($\log(r_e) < 1''.1$) of the cluster.

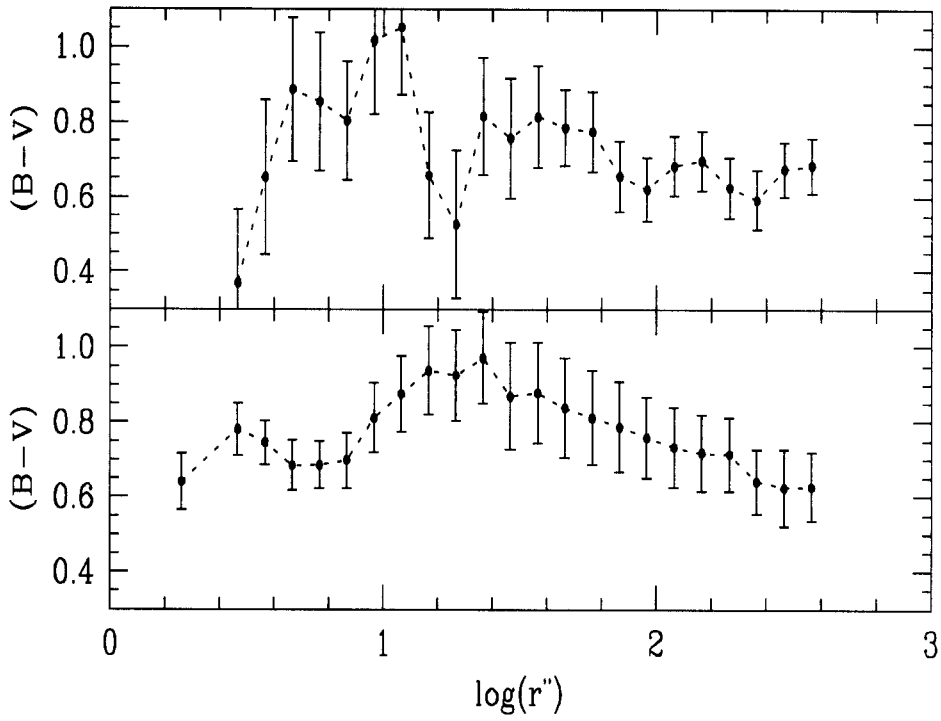


**Figure 5.** Radial $(B - V)$ color distribution of resolved stars on NGC 7089 field (upper panel). The resulting $(B - V)$ color distribution of the star-subtracted image of NGC 7089 is also shown (lower panel).

and $V$ images, we divided the star-subtracted images into eight sectors and concentric annuli of logarithmic radius increments, and measured the median radial $(B - V)$ color distribution. The resulting $(B - V)$ color distribution of star-subtracted images is shown in the lower panel of Figure 5. Columns 4 and 5 of Table 2 list the median radial $(B - V)$ colors and errors of the star-subtracted image. Clearly, no color gradient appears in the central region ($\log(r_e) < 1''.1$) of the cluster. On the other hand, radial color gradient profile of the outer region of the star-subtracted image is very similar to the color gradient from the original $B$ and $V$ images.

## 5. DISCUSSION

Results from the surface photometry and PSF-fitting stellar photometry of NGC 7089 imply that

**Table 2.** Radial $(B-V)$ colors of the resolved stars and the star-subtracted image of the NGC 7089 field.

| [1mm] $\log r_e''$ | $(B-V)_{Stars}$ | $\sigma_{(B-V)_{Stars}}$ | $(B-V)_{bg}$ | $\sigma_{(B-V)_{bg}}$ |
|---|---|---|---|---|
| 0.260 | – | – | 0.640 | 0.075 |
| 0.466 | 0.371 | 0.196 | 0.781 | 0.069 |
| 0.566 | 0.652 | 0.206 | 0.746 | 0.059 |
| 0.666 | 0.887 | 0.192 | 0.684 | 0.067 |
| 0.766 | 0.854 | 0.184 | 0.685 | 0.063 |
| 0.866 | 0.804 | 0.158 | 0.698 | 0.074 |
| 0.966 | 1.018 | 0.198 | 0.811 | 0.093 |
| 1.066 | 1.052 | 0.178 | 0.875 | 0.101 |
| 1.166 | 0.657 | 0.169 | 0.937 | 0.118 |
| 1.266 | 0.527 | 0.197 | 0.925 | 0.121 |
| 1.366 | 0.816 | 0.157 | 0.971 | 0.122 |
| 1.466 | 0.757 | 0.161 | 0.869 | 0.142 |
| 1.566 | 0.814 | 0.135 | 0.878 | 0.135 |
| 1.666 | 0.785 | 0.102 | 0.838 | 0.132 |
| 1.766 | 0.775 | 0.107 | 0.812 | 0.127 |
| 1.866 | 0.655 | 0.095 | 0.787 | 0.120 |
| 1.966 | 0.621 | 0.085 | 0.759 | 0.109 |
| 2.066 | 0.683 | 0.079 | 0.733 | 0.107 |
| 2.166 | 0.697 | 0.080 | 0.717 | 0.102 |
| 2.266 | 0.625 | 0.082 | 0.714 | 0.099 |
| 2.366 | 0.593 | 0.080 | 0.641 | 0.086 |
| 2.466 | 0.675 | 0.073 | 0.625 | 0.103 |
| 2.566 | 0.685 | 0.074 | 0.626 | 0.092 |

the color gradient of the central region of the cluster is due to the resolved bright stars, while the color gradient of the outer region comes from the unresolved background of the cluster. Indeed, this is very exceptional case in the sense that NGC 7089 shows a radial color gradient in the sense of bluer toward center in the central region, in spite of KM surface brightness distribution.

Worth noting that only 17 stars have been resolved in the central region, composite lights of which show a significant radial $(B-V)$ color gradient. We put these stars on the CMD of NGC 7089 as star-like symbols (Figure 4). It is apparent that these stars do not locate at the evolution tracks for cluster stars, but much brighter than HB stars or even red giant branch (RGB) tip. The $\chi$ values of all of these stars are also larger than $\sim 1.3$. These would indicate that even the resolved stars in the very central region of the cluster were fairly contaminated by the crowding effect. We speculate that these stars, which are located at the intermediate position of RGB and HB on CMD, are combinations of RGB stars and blue HB stars of NGC 7089. For example, a combination of a blue HB star of

$V = 16.0$ and $(B - V) = 0.1$ and the other RGB of $V = 16.0$ and $(B - V) = 0.8$ makes a blended star of $V = 15.3$ and $(B - V) = 0.39$. We carefully conclude that the color gradient in the central region of NGC 7089 is due to the light distribution of bright blended stars which are combinations of RGB stars and blue HB stars.

The central region of NGC 7089 seems to be well relaxed system comparing the relaxation time scales, i.e., $\log t_{rc} \sim 8.65$ and $\log t_{rh} \sim 9.05$ years (Djorgovski 1994) with the age of the cluster (cf. Lee & Carney 1999). This leads the mass segregation effect in the central region of the cluster that massive RGB stars are more concentrated than the HB stars which are progenies of RGB stars after mass loss. Our result, however, indicates that there would be an inverse mass segregation effect in the central region of the NGC 7089, if the color gradient is attributed to the differences in distributions of bright blue HB and RGB stars. There were evidences for this unexpected inverse mass segregation phenomenon before. The CMD for M30, which shows a color gradient, from Piotto et al (1988) indicates that there are no excess of bright blue stars near the cluster center, but rather that there is a deficiency of RGB stars. Djorgovski et al. (1991a) also concluded that the color gradients in PCC clusters largely caused by the depletion of RGB and/or subgiants near centers of PCC clusters. We note, however, that there appears to be several different prominence in different clusters, mostly in PCC clusters, related to the radial color gradients (see Djorgovski & Piotto 1993 for detail). In some clusters, e.g., M 15, the gradients seem to be due to mainly the unresolved faint stars (Bailyn et al. 1989, Cederbloom et al. 1992). In others, e.g., NGC 6397, there are color gradients in the light from both bright and faint stars (Lauzeral et al. 1992). Color gradients in the far-UV, which are entirely due to some centrally concentrated hot stellar population, are also seen in some clusters, e.g., M 15, M 30 (Dupree et al. 1979, Djorgovski & Piotto 1992).

We also note that the core morphology of surface brightness distribution, i.e., a power law cusp or a flat core, is not a perfect indicator of the color and population gradients within globular clusters. For example, there is an evidence of significant color gradient in NGC 4147, whose core morphology shows a flat core (Djorgovski et al. 1988, Auriere & Lauzeral 1991). Among other KM clusters, $\omega$ Cen (NGC 5139) and 47 Tuc (NGC 104) show population gradients of hot subdwarfs and blue straggler stars in the central region of the clusters (Guhathakurta et al. 1991, Paresce et al. 1991, Bailyn et al. 1992). Moreover, there are some KM clusters which seem to show color gradients in the far-UV (Dupree et al. 1979).

Sohn et al. (1996) suggested that the color gradients within globular clusters may have a common cause which tends to develope a blue tail in HB morphology, even though their surface brightness distributions can be described by the isothermal King (1966) models. As shown in Figure 4, the CMD of NGC 7089 also shows a well defined blue tail of HB. Fusi Pecci et al. (1993) found that morphology of the HB is correlated with the cluster central density and concentration, in the sense that dense and more concentrated clusters tend to have more extended HB with faint blue tails. This implies that the cluster enviornment can affect the stellar evolution toward the HB stage. Additionally, the interpretation of HB blue tails and HB gaps in CMDs of globular clusters are current hot issues related to the stellar evolution at the He burning stage (Catelan et al. 1998, Ferraro et al. 1998 for detail). All clusters with extreme blue tails found to date have indistinguishable [Fe/H] which is close to $\sim -1.5$. Refer to the metallicity of NGC 7089 as [Fe/H]$= -1.58$ (Djorgovski 1993). Clusters with an extended blue HB tail also show gaps whose physical origin is still mystery. Grundahl et al.

(1999) detected a ubiquitous nature of the jump in Strömgren $u$, so called $u-jump$, from $u$ and $y$ photometry of fourteen globular clusters, which seems to be closely related to the gravity jump and radiative levitation of elements heavier than carbon and nitrogen at $T_{eff} \geq 11,500K$. Indeed, all of these processes may modify stars or at least substantially affect the evolution of HB stars, and therefore the radial population variation and a consequent color gradient.

In conclusion, a significant $(B-V)$ color gradient in the sense of bluer toward cluster center in the central region of NGC 7089, which has a flat core KM surface brightness profile, is mainly due to the combination of RGB stars and blue HB stars. This seems to be related depletion of the RGB stars and/or the ambiguous HB star evolution in the central region of the cluster. The color gradient of the outer region comes from the unresolved background of the cluster, which is mostly composed of faint stars in the cluster. We caution, however, to confirm the reality of the color gradient from resolved stars, we need more accurate imaging data of the cluster with exceptional seeing condition because the effect of completeness correlates with local density of stars.

## 6. SUMMARY

We have used $BV$ CCD images to investigate the color gradient within a globular cluster NGC 7089. The surface brightness distribution of the cluster follows an isothermal King (1966) model with a flat core. A strong radial color gradient in the central region of the cluster, in the sense of bluer center, was confirmed with the amplitude of $\sim 0.39 \pm 0.07$ mag/arcsec$^2$ in $(B-V)$. In the outer region of the cluster, however, the radial color gradient shows a reverse case, i.e., redder toward the center with the amplitude of $\sim -0.18 \pm 0.01$ mag/arcsec$^2$. $(B-V)$ color profile of resolved stars in the NGC 7089 field also shows a strong color gradient in the central region of the cluster, which implies that the combination of RGB stars and blue HB stars causes the color gradient. The depletion of the RGB stars in the central region of NGC 7089 and/or an ambiguous evolutionary effect of HB stars have been suggested to explain the radial color gradients in the central region of the cluster. Color gradient of the outer region of NGC 7089 may be due to the unresolved background of the cluster.

**ACKNOWLEDGMENTS:** This paper is supported in part by Creative Research Initiatives of the Korean Ministry of Science and Technology. M.S.C. acknowledges support from the Basic Science Institute Program (BSRI 1998-015-D00287), Ministry of Education.

## REFERENCES

Auriere, M. & Cordoni, J.P. 1983, A&AS, 51, 135
Auriere, M. & Lauzeral, C. 1991, A&A, 244, 303
Bailyn, C., Grindlay, J., Cohn, H., Lugger, H., Stetson, P., & Hesser, J. 1989, AJ, 98, 882
Bailyn, C., Sarajedini, A., Cohn, H., Lugger, H., & Grindlay, J. 1992, AJ, 103, 1564

Bolte, M. 1989, ApJ, 341, 168
Catelan, M., Borissova, J., Sweigart, A.V., & Spassova, N. 1998, ApJ, 494, 265
Cederbloom, S., Moss, M., Cohn, H., Lugger, P., Bailyn, C., Grindlay, J., & McClure, R. 1992, AJ, 103, 480
Cudworth, K. & Rauscher, B.J. 1987, AJ, 93, 856
Djorgovski, S. 1993, in ASPCS vol. 50, Structure and Dynamics of Globular Clusters, ed. S.G. Djorgovski & G. Meylan, (San Fransisco: Astronomical Society of the Pacific), 373
Djorgovski, S. & Piotto, G. 1992, AJ, 104, 2112
Djorgovski, S. & Piotto, G. 1993, in ASPCS vol. 48, Globular Cluster Galaxy Connection, ed. G.H. Smith & J.P. Brodie, (San Fransisco: Astronomical Society of the Pacific), 84
Djorgovski, S., Piotto, G., & King, I.R. 1988, Dynamics of Dense Stellar Systems, ed. D. Merritt, (Cambridge: Cambridge University Press), 147
Djorgovski, S., Piotto, G., & Mallen-Ornelas, G. 1991a, in ASPCS vol. 13, Formation and Evolution of Star Clusters, ed. K. Janes, (San Fransisco: Astronomical Society of the Pacific), 262
Djorgovski, S., Piotto, G., Phinney, E.S., & Chernoff, D.F. 1991b, ApJ, 372, L41
Drukier, G.A., Fahlman, G.G., Richer, H.B., & Chernoff, D.F. 1993, in ASPCS vol. 48, Globular Cluster Galaxy Connection, ed. G.H. Smith & J.P. Brodie, (San Fransisco: Astronomical Society of the Pacific), 88
Dupree, A., Hartmann, L., Black, J., Davis, R., Matisky, T., Raymond, J., & Gursky, H. 1979, ApJ, 230, L89
Ferraro, F.R., Paltrinieri, B., Fusi Pecci, F., Rood, R.T., & Dorman, B. 1998, ApJ, 500, 311
Fusi Pecci, F., Ferraro, F.R., Bellazzini, M., Djorgovski, S., Piotto, G., & Buonanno, R. 1993, AJ, 105, 1145
Grindlay, J.E., Hertz, P., Steiner, J.E., Murray, S.S., & Lightman, A.P. 1984, ApJ, 282, L13
Grundahl, F., Catelan, M., Landsman, W.B., Stetson, P.B., & Andersen, M.I. 1999, ApJ, submitted
Guhathakurta, P., Yanny, B., Schneider, D., & Bahcall, J. 1992, A&A, 262, 63
Harris, W.E. 1975, ApJS, 29, 397
King, I.R. 1966, AJ, 71, 64
Landolt, A.U. 1992, AJ, 104, 340
Lauzeral, C., Auriere, M., Ortolani, S., & Melnick, J. 1992, A&A, 262, 63
Lee, J.W. & Carney, B.W. 1999, AJ, in press
Lee, M.G. 1990, PhD thesis, University of Washington
Leonard, P.J.T. 1989, AJ, 98, 217
Nemec, J.M. & Harris, H.C. 1987, ApJ, 316, 172
Nemec, J.M. & Cohen, J.G. 1989, ApJ, 336, 780
Parsce, F., et al. 1991, Nature, 352, 297
Peterson, C.J. 1986, PASP, 98, 192
Piotto, G., King, I.R., & Djorgovski, S. 1988, AJ, 96, 1918
Richer, H.B. & Fahlman, G.G. 1989, ApJ, 339, 178
Sohn, Y.J., Byun, Y.I., & Chun, M.S. 1996, Ap&SS, 243, 379
Stetson, P.B. 1987, PASP, 99, 191
Stetson, P.B. 1995, DAOPHOT II User's Manual

Stetson, P.B. & Harris, W.E. 1988, AJ, 96, 909
Zinn, R. 1985, ApJ, 293, 424